Solution Structures and Backbone Dynamics of *Escherichia coli* Rhodanese PspE in Its Sulfur-Free and Persulfide-Intermediate Forms: Implications for the Catalytic Mechanism of Rhodanese[†,‡]

Hongwei Li,[§,||] Fan Yang,[§,||] Xue Kang,[§,||] Bin Xia,[§,||,⊥] and Changwen Jin*[,§,||,⊥]

Beijing Nuclear Magnetic Resonance Center, and College of Chemistry and Molecular Engineering, and College of Life Sciences, Peking University, Beijing 100871, China

Received January 8, 2008; Revised Manuscript Received February 22, 2008

ABSTRACT: Rhodanese catalyzes the sulfur-transfer reaction that transfers sulfur from thiosulfate to cyanide by a double-displacement mechanism, in which an active cysteine residue plays a central role. Previous studies indicated that the phage-shock protein E (PspE) from *Escherichia coli* is a rhodanese composed of a single active domain and is the only accessible rhodanese among the three single-domain rhodaneses in *E. coli*. To understand the catalytic mechanism of rhodanese at the molecular level, we determined the solution structures of the sulfur-free and persulfide-intermediate forms of PspE by nuclear magnetic resonance (NMR) spectroscopy and identified the active site by NMR titration experiments. To obtain further insights into the catalytic mechanism, we studied backbone dynamics by NMR relaxation experiments. Our results demonstrated that the overall structures in both sulfur-free and persulfide-intermediate forms are highly similar, suggesting that no significant conformational changes occurred during the catalytic reaction. However, the backbone dynamics revealed that the motional properties of PspE in its sulfur-free form are different from the persulfide-intermediate state. The conformational exchanges are largely enhanced in the persulfide-intermediate form of PspE, especially around the active site. The present structural and biochemical studies in combination with backbone dynamics provide further insights in understanding the catalytic mechanism of rhodanese.

Rhodanese (thiosulfate:cyanide sulfertransferase or TST,[1] EC 2.8.1.1) is a large superfamily of enzymes commonly found in bacterial, archeal, and eukaryotic cells. These enzymes catalyze the sulfur-transfer reaction in which a sulfur atom is transferred from thiosulfate to cyanide (*1*–*8*). The catalytic reaction occurs through a double-displacement mechanism, in which a conserved cysteine residue plays a central role (*9*). Briefly, in the first step of the reaction, the sulfhydryl group of the active cysteine residue of rhodanese attacks the thiosulfate anion to form an enzyme-persulfide intermediate. Subsequently, the persulfide intermediate of the enzyme is attacked by the cyanide ion to release the thiocyanide and sulfite ions, completing one cycle of sulfur transfer. Meanwhile, the rhodanese returns to its active form for the next round of catalysis. On the basis of the sequence, domain arrangement, and active loop length, the rhodanese superfamily can be classified into four major groups: single-domain proteins, tandem-domain proteins, multidomain proteins, and elongated active-site loop proteins (*9*). Most typical rhodaneses belong to the tandem- or single-domain rhodaneses. Despite the variety of sequences, all of the tandem-domain rhodaneses are composed of two domains with the same fold, the inactive N-terminal domain and the catalytic C-terminal domain. The catalytic C-terminal domain contains the conventional six-residue active loop beginning with the essential cysteine residue. In the inactive N-terminal domain, the active cysteine residue is replaced by an aspartic acid residue at the corresponding position (*9, 10*). The single-domain rhodaneses contain only one domain, either active or inactive. Currently, several rhodanese structures are reported (*11*–*16*). Among these, the crystal structures of the bovine rhodanese Rhobov (*11*) and the *Escherichia coli* GlpE (*13*) represent the prototypes of tandem- and single-domain rhodaneses, respectively.

Previous studies on *E. coli* demonstrated two distinct rhodanese activities. One was detectable using intact cell (the accessible rhodanese), while the other was released only after

[†] This work was supported by Grant 2006CB910203 from the National Basic Research Program and Grant 2006AA02A323 from the National High Technology Research and Development Program of China (to C.J.).

[‡] The atomic coordinates and structure factors (PDB codes 2JTQ and 2JTR) have been deposited in the Protein Data Bank (PDB), Research Collaboratory for Structural Bioinformatics, Rutgers University, New Brunswick, NJ (http://www.rcsb.org/).

* To whom correspondence should be addressed. Telephone: +86-10-6275-6004. Fax: +86-10-6275-3790. E-mail: changwen@pku.edu.cn.

[§] Beijing Nuclear Magnetic Resonance Center.

[||] College of Chemistry and Molecular Engineering, Peking University.

[⊥] College of Life Sciences, Peking University.

[1] Abbreviations: PspE, phage-shock protein E; NMR, nuclear magnetic resonance; TST, thiosulfate:cyanide sulfertransferase; GlpE, *sn*-glycerol 3-phosphate E; IPTG, isopropyl-β-D-thiogalactoside; DSS, 2-dimethyl-2-silapentanesulfonic; HSQC, heteronuclear single-quantum coherence; 2D (3D), two (three) dimensional; COSY, correlation spectroscopy; TOCSY, total correlation spectroscopy; DTT, 1,4-dithiothreitol; NOE, nuclear Overhauser effect; rmsd, root-mean-square deviation.

10.1021/bi800039n CCC: $40.75
Published on Web 03/21/2008

the cells were sonicated (*3*). The accessible rhodanese was identified to be a periplasmic protein with an apparent molecular weight of about 12–14 kDa, corresponding to the size of a single-domain rhodanese (*17*). The *E. coli* genome consists of eight genes encoding proteins with rhodanese domains, three of which (GlpE, PspE, and YgaP) belong to the single-domain family (*13*). Among them, PspE is the only rhodanese with a N-terminal signal peptide (the first 19 residues in the sequence) and corresponds to the accessible rhodanese (*17*). A previous study indicated that the enzymic activity of PspE is 2 orders of magnitude higher than that of GlpE, a cytoplasmic rhodanese in *E. coli* (*17*).

The *pspE* gene belongs to the *psp* (*phage-shock protein*) operon, which shows induced expression under stress conditions (*17–22*). However, the function of PspE does not appear directly related to the other Psp proteins (*18*). PspE consists of 104 residues, and the N-terminal 19 residues are the signal peptide. The sequence of PspE shows good similarity to GlpE (26% identity and 44% similarity over 72 aligned residues). In addition, the sequence length of PspE (85 residues) is significantly shorter than that of GlpE (108 residues). To shed light on the function of PspE, especially the structural basis of its enzymic activity, we determined the solution structures of the sulfur-free and persulfide-intermediate forms of PspE using nuclear magnetic resonance (NMR) spectroscopy.

It is commonly accepted that the internal dynamics plays a central role in the function of proteins, especially enzymatic catalysis (*23–26*). NMR spectroscopy is uniquely suited to study the protein dynamics at atomic resolution (*23*). To obtain further insights into the catalytic mechanism of the rhodanese, we investigated the backbone dynamics of PspE in both sulfur-free and persulfide-intermediate forms. The structures in combination with the backbone dynamics provide the molecular and dynamic basis in understanding the mechanism of the rhodanese-catalyzed sulfur-transfer reaction.

MATERIALS AND METHODS

Cloning and Protein Expression. The complete *E. coli pspE* gene, including the N-terminal sequence coding for the signal peptide, was cloned into the pET21a(+) vector and expressed in *E. coli* BL21 (DE3) strain (Novagen). The restriction sites *Nde* I and *Eco*R I were used, and a stop codon was added at the C terminus of the gene. Therefore, no additional tag sequences were contained in the recombinant protein. The cell culture was grown in 500 mL of Luria-Bertani medium with ampicillin. When OD_{600} reached 0.8, the cells were centrifuged and resuspended in 250 mL of M9 minimal medium at 25 °C. For the production of $^{13}C/^{15}N$- or ^{15}N-labeled samples, $^{15}NH_4Cl$ and $^{13}C_6$ glucose or only $^{15}NH_4Cl$ was used in the medium (*27*). Protein expression was induced by isopropyl-β-D-thiogalactoside (IPTG) at a final concentration of 100 mg/L. The cells were harvested 10 h after induction at 25 °C. PspE was purified using anion-exchange chromatography (Mono Q) and subsequently the gel filtration (superdex-75) with an ÄKTA FPLC system (Amersham Biosciences).

NMR Sample Preparations. The sulfur-free PspE was prepared in a buffer containing 30 mM sodium phosphate and 40 mM 1,4-dithiothreitol (DTT) in 90% H_2O/10% D_2O (pH 7.2). The protein concentration was about 1 mM. For preparation of the persulfide-intermediate form of PspE, DTT was removed from the sample by buffer exchange using 20 mM Tris-HCl and 20 mM of sodium thiosulfate was subsequently added. All samples were argon-flushed.

NMR Spectroscopy. The NMR experiments were performed at 25 °C on Bruker Avance 500, 600, and 800 MHz spectrometers equipped with four RF channels and triple-resonance probes with pulsed-field gradients. 2-Dimethyl-2-silapentanesulfonic (DSS) was used as the internal chemical-shift reference. The chemical-shift assignments of backbone and side-chain atoms were obtained by two-dimensional (2D) ^{15}N- and ^{13}C-edited heteronuclear single-quantum coherence (HSQC) experiments and three-dimensional (3D) HNCA, HNCO, HNCACB, HBHA(CO)NH, CBCA(CO)NH, (H)CC-(CO)NH, (H)CCH-COSY, and (H)CCH-TOCSY experiments (*28–33*). Three-dimensional (3D) ^{15}N- and ^{13}C-edited NOESY-HSQC spectra (mixing time of 100 ms) were collected to confirm the chemical-shift assignments and generate distance restraints for structure calculations (*34*). The NMR spectra were processed using NMRPipe (*35*) and analyzed by NMRView (*36*).

Structure Calculations. The distance restraints derived from interproton nuclear Overhauser effect (NOE) and dihedral angles (φ, ψ) from chemical shifts by TALOS (*37*) were used to calculate the PspE structures. The structures were calculated using CYANA (*38*) and refined using AMBER (*39*). The CANDID module of the CYANA program (*38, 40*) was used to generate the initial structures, from which the 20 lowest energy structures were selected to extend the NOE assignments by SANE (*41*). A total of 200 structures were calculated by CYANA, and 100 structures with the lowest energy were selected as the initial structures for refinements using AMBER. Finally, the 20 lowest energy conformers were selected to represent the solution structures of PspE in each form. The final structures were analyzed using MOLMOL (*42*) and PROCHECK_NMR (*43*).

Titration Experiments of Thiosulfate. PspE was dissolved in the buffer used for the intermediate-structure determination. The titration experiments were performed at pH 7.2 and monitored by 2D ^{15}N-edited HSQC experiments. The molar ratio of the thiosulfate/protein ranged from 1 to 20.

Backbone ^{15}N Relaxation Measurements. The backbone ^{15}N relaxation parameters of longitudinal relaxation rates (R_1), transverse relaxation rates (R_2), and steady-state heteronuclear $\{^1H\}-^{15}N$ NOE values of the sulfur-free and persulfide-intermediate forms of PspE were measured in Tris-HCl buffer on the Bruker Avance 800 MHz spectrometer at 25 °C (*44*). The spectral widths for ^1H and ^{15}N were 11160.7 and 2432.8 Hz, respectively. For the R_1 and R_2 measurements, 1024 (^1H) and 68 (^{15}N) complex data points were collected with 16 transients and a recycle delay of 3 s. The delays used for R_1 experiments were 10 (×2), 100, 300, 700, 1200, 1700, 2300, 2900 and 3490 ms, and those used for the R_2 measurements were 8 (×2), 16, 32, 52, 76, 116, 164, 220, and 280 ms. The relaxation rate constants were obtained by fitting the peak intensities to a single exponential function using the nonlinear least-squares method (*45*). The $\{^1H\}-^{15}N$ NOE experiments were performed in the presence and absence of a 3 s proton presaturation period prior to the ^{15}N excitation

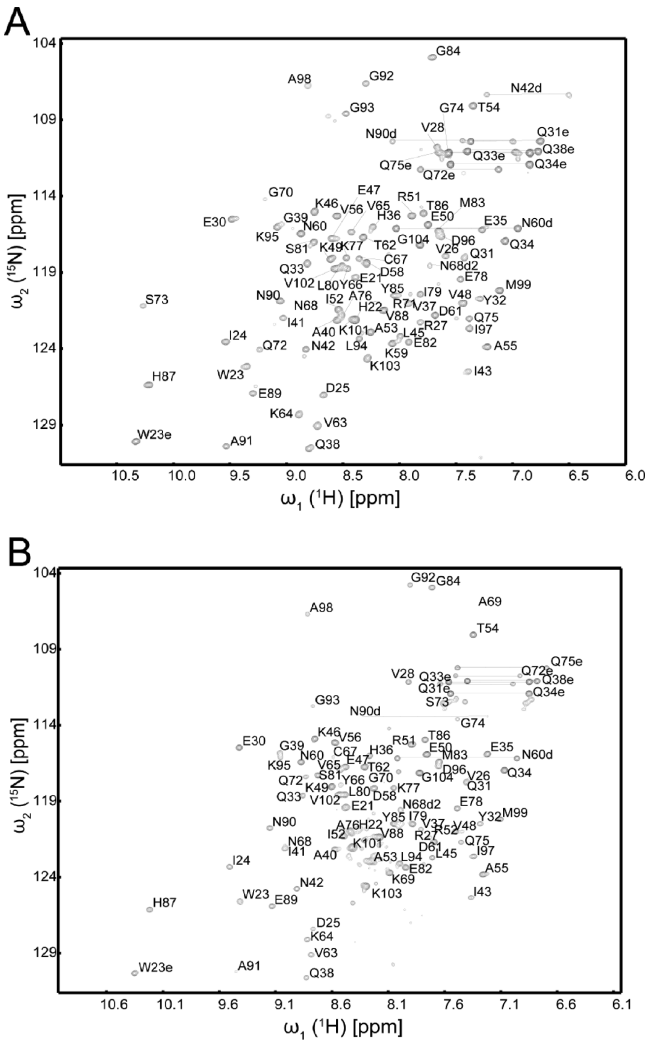

FIGURE 1: Two-dimensional ^{15}N-edited HSQC spectra annotated with the backbone assignments of rhodanese PspE in both sulfur-free (A) and persulfide-intermediate (B) forms at pH 7.2. The assignments were labeled with the one-letter amino acid code and residue number.

pulse and using recycle delays of 3 and 6 s (*45*). A total of 32 transients were used in each experiment.

RESULTS AND DISCUSSION

Chemical-Shift Assignments and Characterization of PspE. The first 19 residues of PspE constitute the signal peptide, and they are cleaved during recombinant expression in *E. coli*. Therefore, the sequence of PspE samples used in this study corresponds to residues Ala20−Gly104 of PspE. For PspE in both the sulfur-free and persulfide-intermediate forms, chemical shifts were assigned for more than 99% of the atoms. The 2D ^{15}N-edited HSQC spectra annotated with the backbone assignments for both forms of PspE are shown in Figure 1.

The HSQC spectra of both forms of PspE showed a single set of well-dispersed peaks, indicating homogeneous conformations. The C_β chemical shift of Cys67 was 25.5 ppm in sulfur-free PspE, while it was 39.5 ppm after incubation with sodium thiosulfate (see the Materials and Methods). Because PspE contains only one cysteine residue, the formation of the intramolecular disulfide bond is impossible. Furthermore, experimental results from sodium dodecyl sulfate-polyacrylamide gel electrophoresis (SDS-PAGE), mass spectroscopy, and gel filtration demonstrated the monomeric state of PspE in both forms (data not shown), excluding the possibility of intermolecular disulfide bond formation. These results in combination with previous studies of rhodaneses (*3, 13, 17, 46*) indicate the formation of a PspE persulfide intermediate.

In addition, to investigate which form of PspE was produced during recombinant expression, we directly purified ^{15}N-labeled PspE without DTT treatment and obtained its HSQC spectrum (see the Supporting Information). The spectrum was identical to that of the DTT-treated sample but distinct from the sodium thiosulfate incubated one. This result indicates that the PspE produced during overexpression in *E. coli* exists in the sulfur-free form.

Solution Structures of PspE. The solution structures of PspE in both forms were calculated using the interproton distance restraints derived from 3D ^{15}N- and ^{13}C-edited NOESY-HSQC experiments and the dihedral angle restraints based on chemical shifts predicted by TALOS (*37*). The lowest energy conformers (20 for each form) were selected to represent the structures of PspE in the sulfur-free and persulfide-intermediate forms, respectively. The structural ensemble of 20 representative structures and the ribbon diagram of the energy-minimized mean structure of PspE in each form are shown in parts A and B of Figure 2. The structural statistics are summarized in Table 1.

The structures of the sulfur-free and persulfide-intermediate forms of PspE are highly similar. The backbone root-mean-square deviation (rmsd) between the mean structures of the two forms is 0.97 Å for all residues and 0.90 Å for residues in regular secondary structures. Both structures consist of six β strands (residues: Glu21−Asp25, β1; Glu35−Val37, β2; Ile41−Asn42, β3; Thr62−Cys67, β4; Val88−Gly93, β5; and Lys101−Lys103, β6) and three α helices (Pro29−Tyr32, α1; Leu45−Ala55, α2; and Arg71−Glu82, α3), forming a typical single α/β rhodanese domain. The four β strands β1, β3, β4, and β5 constitute a central parallel twisted β sheet, with a topology of 3–1–4–5 (Figure 2C). Helices α2 and α3 are packed on one side of the β sheet, while the short helix α1 is packed on the other side. In addition, β2 and β6 form an antiparallel β sheet, which may stabilize the C-terminal segment of PspE as similarly suggested for GlpE (*13*).

The HSQC spectrum of the persulfide-intermediate form of PspE showed a lower quality than that of the sulfur-free form. Additionally, there were fewer observable NOEs (a total of 2754) compared to the sulfur-free form (a total of 3279). As a consequence, the backbone rmsd value of the persulfide-intermediate form is higher than the sulfur-free form. However, the persulfide-intermediate form of PspE was biochemically stable, and the sample kept unchanged during the NMR spectra collection for structure determinations. The apparent lower spectra and structural quality of the persulfide form of PspE is mostly caused by conformational exchanges (see the Internal Dynamics section).

Active Site of PspE. To confirm the active site of PspE, we performed sodium thiosulfate titration experiments monitored by 2D ^{15}N-edited HSQC spectra. Figure 3A shows the chemical-shift differences between the sulfur-free and persulfide-intermediate forms of PspE. Two regions show large chemical-shift differences. The first region showing

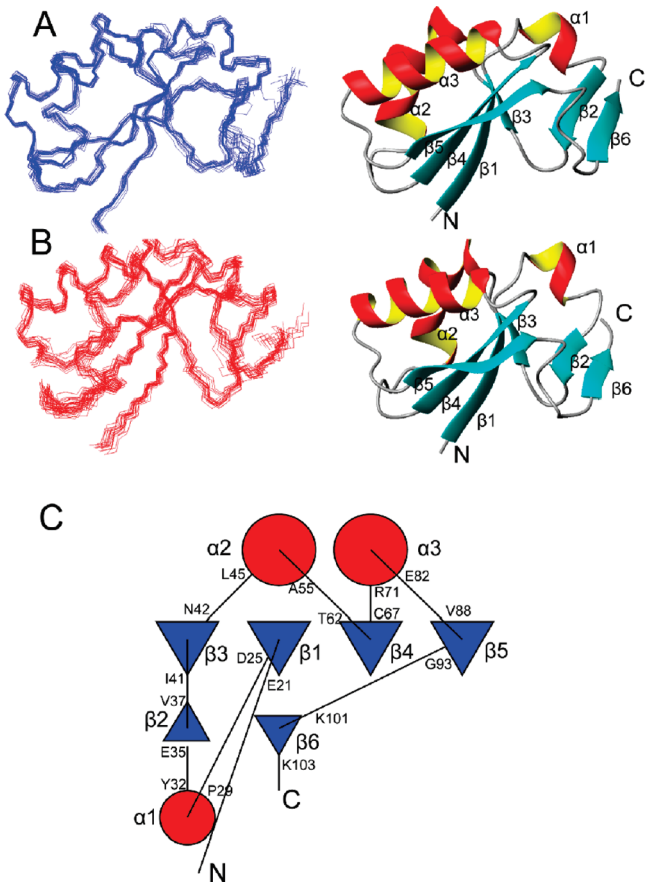

FIGURE 2: Solution structures and topology diagram of rhodanese PspE in the sulfur-free and persulfide-intermediate forms. (A) Superimposition of the 20 representative structures of sulfur-free PspE (left) and ribbon diagram of the mean structure (right). The secondary-structural elements are labeled. (B) Superimposition of the 20 representative structures of persulfide-intermediate PspE (left) and ribbon diagram of the mean structure (right). The figures were generated using MOLMOL (*42*). (C) Topology diagram of PspE generated via the TOPS website (www.tops.leeds.ac.uk) (*53*). The α helices are in red, and the *β* strands are in blue. The residues at the start and end of the secondary structures are labeled with the one-letter amino acid codes and residue numbers.

larger chemical-shift differences contains residues Cys67−Gly74, corresponding to the active site of PspE (Figure 3B). This result is in agreement with previous characterizations of rhodanese active sites (*11*–*13*). The second region consists of residues Gly92−Leu94, which is structurally adjacent to the active site (Figure 3B).

The active site of PspE (residues Cys67−Gln72) links *β*4 and α3. The active Cys67 is the last residue of *β*4, and residues Arg71 and Gln72 form the first turn of α3. The loop between *β*4 and α3 is composed of only three residues Asn68, Ala69, and Gly70. Similar to other rhodaneses, the active-site residues of PspE form a semicircular cradle-like conformation (*11*–*13*). The side-chain S_γ atom of Cys67 in PspE locates at the center of the cradle (Figure 3B), and most of the backbone amides of residues Asn68−Gln72 point toward it. The distances between the S_γ atom of Cys67 and the amide hydrogen atoms of residues Asn68, Ala69, Gly70, Arg71, Gln72, and Ser73 are 2.8, 2.7, 2.3, 4.0, 2.9, and 2.8 Å in the mean structure of the sulfur-free form of PspE. In contrast, the corresponding distances are 3.5, 4.5, 2.6, 3.3, 2.6, and 2.8 Å in the mean structure of the persulfide-intermediate form of PspE. In addition, the side-chain hydroxyl group of Ser73 is also in proximity to the S_γ atom of Cys67 in both forms of PspE (3.8 Å in sulfur-free PspE and 3.5 Å in persulfide-intermediate form). These results suggest that the active sulfur atom in PspE is likely involved in a radial hydrogen-bonding network, which may contribute to the stabilization of the active site of both forms of PspE, as similarly observed in other rhodaneses (*11*, *13*). Notably, the distances between S_γ and the amide hydrogen atoms of active-loop residues (Asn68, Ala69, and Gly70) become larger in the persulfide-intermediate form of PspE than that of the sulfur-free form. This may suggest an increasing of the motional flexibility of the active Cys67 in the persulfide-intermediate form of PspE, which will be discussed below.

Structural Comparisons. The overall structures of PspE in both forms are highly similar to other rhodanese domains. A DALI search (*47*) showed that PspE has the highest structural homology with *E. coli* GlpE. Both PspE and GlpE belong to the single-domain rhodaneses with one active cysteine residue. The rmsd of C_α atoms is only 1.8 Å for 82 aligned residues between the two structures. As shown in Figure 4A, two major structural differences were observed. First, the N-terminal 19 residues of GlpE form the first α helix and *β* strand (designated as α0 and *β*0 in this paper) in its structure, while PspE lacks the corresponding region. Secondarily, in the C-terminal region of the PspE structure, the segment between *β*5 and *β*6 contains fewer residues (Leu94−Pro100) and forms a loop conformation. In contrast, the corresponding segment (Asp90−Glu103) of GlpE is longer and forms a well-defined α helix (designated as α4 in this paper). Therefore, PspE lacks two α helices and one *β* strand compared to GlpE. A close inspection on structures of rhodaneses solved to date shows that all structures contain α0 and *β*0 except for PspE. On the other hand, some rhodaneses, such as PspE, adopt a looplike conformation in the region corresponding to α4 in GlpE. In addition, structural comparisons indicate that other rhodanese domains mostly contain long loops connecting regular secondary-structural elements, while in PspE, the loops are much shorter. Taken together, the structure of PspE represents a minimized rhodanese domain with the shortest length of sequence and the fewest secondary-structural elements.

The active-site conformation of PspE is similar to that of other rhodaneses. The main difference is that the active cysteine residue Cys67 is the last residue of the strand *β*4, instead of the first residue of the active loops observed in other rhodaneses. In addition, the loop segment of the active site in PspE contains only three residues, which is shorter than that of other rhodaneses. The comparison of the active site of PspE and GlpE is shown in Figure 4B.

There are several highly conserved residues among rhodaneses, such as Asp25, Arg27, His36, Gly84, Val88, Gly93, and Pro100 (numbered according to PspE sequence), suggesting they may play important roles in either maintaining structural integrity or function in enzymatic catalysis. By comparing the structures of PspE in the sulfur-free and persulfide-intermediate forms, we found that none of these residues show conformational changes between the two states. Among these, residues Gly84 and Pro100 are both in loop regions and located far from the active site, suggesting their possible roles in the formation of turns. Residue Val88 is also away from the active site, and its side chain is buried inside the protein, suggesting its role in forming the structural

Table 1: Structural Statistics of *E. coli* Rhodanese PspE

	sulfur-free	persulfide-intermediate
distance restraints		
intraresidue unambiguous NOEs	928	834
sequential unambiguous NOEs	479	382
medium-range unambiguous NOEs	267	234
long-range unambiguous NOEs	533	346
total unambiguous NOEs	2207	1796
total ambiguous NOEs	1072	958
dihedral angles (φ and ψ)	54	68
rmsd from mean structure (Å)		
secondary-structure backbone atoms	0.33 ± 0.06	0.44 ± 0.06
secondary-structure heavy atoms	0.62 ± 0.11	0.67 ± 0.08
all backbone atoms	0.45 ± 0.10	0.55 ± 0.09
all heavy atoms	0.67 ± 0.11	0.78 ± 0.08
energy (kcal/mol)		
mean amber energy	−4578.93 ± 8.10	−4581.45 ± 7.23
NOE distance restraints violation energy	8.85 ± 1.17	4.85 ± 0.77
torsion angle restraints violation energy	0.48 ± 0.14	0.84 ± 0.21
restraint violations		
distance (>0.3 Å)	0	0
dihedral angle (>5°)	1	0
Ramachandran statistics (%)		
residues in most favored regions	85.0	84.6
residues in additional allowed regions	14.6	15.1
residues in generously allowed regions	0.4	0.3
residues in disallowed regions	0.0	0.0

core of rhodaneses. Residues Asp25, Arg27, His36, and Gly93 are all spatially clustered near the active site. Residues Asp25 and Arg27 are located adjacent to the active cysteine, and the side chains of these two residues are in close contact with each other, suggesting an electrostatic interaction. This conformation is similarly found in other rhodanese structures (*11–13*). Residue His36 locates on β2, and its side chain interacts with the aromatic side chain of Tyr32 on α1. In other rhodaneses, the corresponding histidine also interacts with an aromatic residue (Phe32 in GlpE, Tyr187 in bovine rhodanese, and Tyr174 in *Azotobacter vinelandii* rhodanese). These observations strongly suggest that residues Asp25, Arg27 and His36 are essential for maintaining the local conformation and chemical environment near the active pocket. On the other hand, the conserved residue Gly93 might be important for providing conformational flexibility for the enzymatic catalysis and will be discussed below.

Relaxation Parameters. To investigate the internal dynamics of PspE and obtain further insights into the molecular mechanism of rhodanese catalysis, we measured the backbone ^{15}N longitudinal relaxation rates (R_1), transverse relaxation rates (R_2), and heteronuclear {^{1}H}-^{15}N NOE values. During the analysis of the relaxation data, 77 and 75 of 85 residues were used for the sulfur-free and the persulfide-intermediate forms of PspE, respectively. The unanalyzed residues included four proline residues that have no amide protons, the unassigned residues, and eight residues that were either overlapped or too weak to be analyzed. The experimentally determined R_1, R_2, and {^{1}H}-^{15}N NOE values versus the amino acid sequence are shown in Figure 5A.

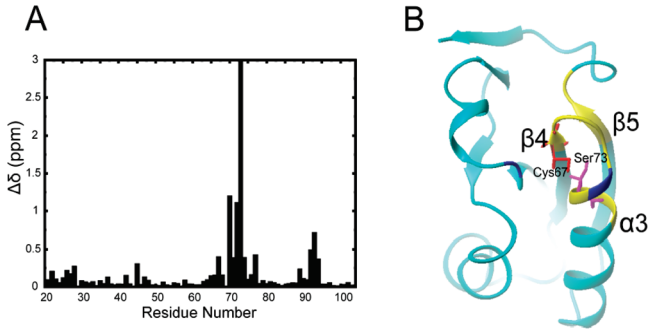

FIGURE 3: Active site of PspE. (A) Chemical-shift differences between sulfur-free and persulfide-intermediate forms of PspE. The composite chemical-shift changes were calculated using the equation $\Delta\delta_{comp} = \sqrt{\Delta\delta_H^2 + (\Delta\delta_N/6)^2}$, where $\Delta\delta_H$ and $\Delta\delta_N$ represent the chemical-shift changes of ^{1}H and ^{15}N, respectively (*54*). (B) Active site of PspE mapped onto the structure. The side chains of Cys67 and Ser73 are shown in red and magenta, respectively. Two segments (residues Cys74−Gly74 and Gly92−Leu94) with larger chemical-shift differences are mapped onto the PspE structure (yellow). The unassigned residue Ala69 is in blue.

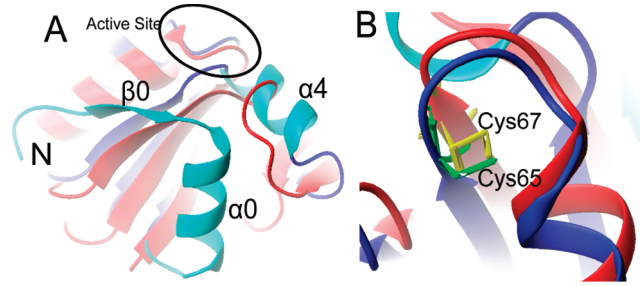

FIGURE 4: Structural comparison between PspE and GlpE. (A) Comparison of the overall structures between PspE and GlpE. The structure of PspE is shown in red, while that of GlpE is shown in blue. For clarity, the α0, α4, and β0 of GlpE are in cyan. The active sites of PspE and GlpE are shown in ellipse. (B) Comparison of the active sites of PspE and GlpE. The active cysteines of PspE and GlpE are shown in yellow and green, respectively.

Overall, PspE in both forms is rigid, as reflected by the {^{1}H}-^{15}N NOE values. Residues in the N and C termini show relatively low NOE values, indicating the motional flexibility on the pico-nanosecond timescales. For both forms of PspE, residues Gln33, Gln38−Gly39, and Val65−Gly74 show larger than average R_2/R_1 values, indicative of conformational exchanges on micro-millisecond timescales and/or motional anisotropy on pico-nanosecond timescales. Moreover, residues Ala91, Gly93, Lys95, and Ala98 in persulfide-intermediate PspE also show high R_2/R_1 ratios. These results are different from the previous relaxation study on *A.*

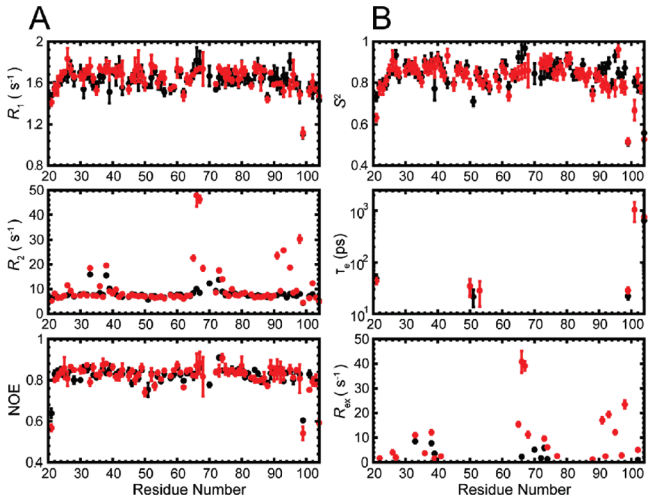

FIGURE 5: Backbone relaxation data and internal mobility parameters of PspE in the sulfur-free and persulfide-intermediate forms. (A) Longitudinal relaxation rates (R_1), transverse relaxation rates (R_2), and heteronuclear {^{1}H}-^{15}N NOE values of sulfur-free PspE (black) and persulfide-intermediate PspE (red) versus the amino acid sequence. The experiments were performed on a Bruker Avance 800 MHz spectrometer at 25 °C. Uncertainties were obtained by Monte Carlo simulations. (B) Internal dynamics parameters of generalized order parameter S^2, internal correlation time τ_e, and the conformational exchange R_{ex} versus the amino acid sequence of PspE in the sulfur-free (black) and persulfide-intermediate (red) forms.

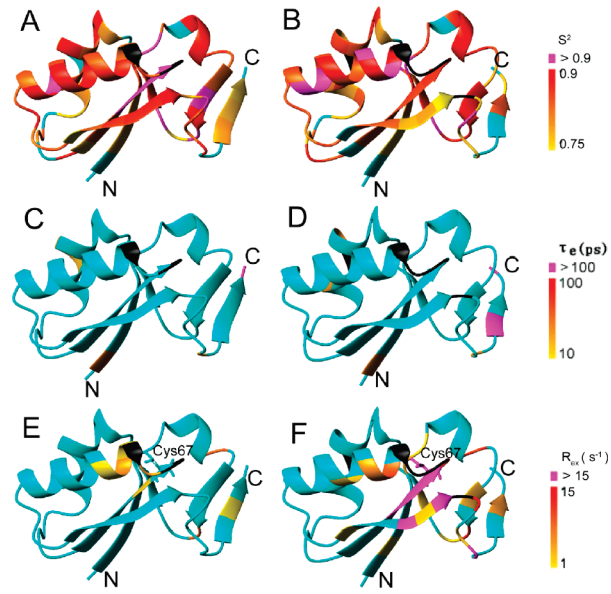

FIGURE 6: Ribbon diagrams representing the dynamic properties of PspE in sulfur-free and persulfide-intermediate forms. (A and B) Ribbon diagrams of the sulfur-free PspE (A) and persulfide-intermediate PspE (B) representing the generalized order parameter S^2 values, with colors ranging from yellow to red and magenta corresponding to S^2 values from 0.75 to 0.9 and >0.9. (C and D) Ribbon diagrams of sulfur-free PspE (C) and persulfide-intermediate PspE (D) representing the internal motion on pico−nanosecond timescales, with colors ranging from yellow to red and magenta corresponding to τ_e values from 10 to 100 and >100 ps. (E and F) Ribbon diagrams of sulfur-free PspE (E) and persulfide-intermediate PspE (F) representing the conformational exchange R_{ex} with colors ranging from yellow to red and magenta corresponding to R_{ex} values from 1 to 15 and >15 s^{-1}.

vinelandii rhodanese, in which the sulfur-free and sulfur-loaded forms showed similar relaxation rates (*48*).

Rotational Diffusion Anisotropy. The ratios of the principal components of the inertia tensors calculated from the solution structures of PspE in sulfur-free and persulfide-intermediate forms are 1:0.94:0.58 and 1:0.91:0.59, respectively. This result suggests a strong motional anisotropy of PspE in both forms. We followed the common procedures to determine the rotational diffusion tensors of PspE in both forms by excluding residues with conformational exchanges and/or internal motions (*49*). A total of 63 and 46 residues were used to determine the rotational diffusion tensors of sulfur-free and persulfide-intermediate forms of PspE, respectively. The diffusion tensors were best defined by the axially symmetric model for both forms, giving the global correlation time $\tau_m = 4.42 \pm 0.02$ and 4.30 ± 0.03 ns and anisotropy of diffusion tensors $D_{\parallel}/D_{\perp} = 1.18 \pm 0.04$ and 1.25 ± 0.05 for sulfur-free and persulfide-intermediate forms, respectively. The correlation times indicate that both forms of PspE are in the monomeric state, which is in accordance with the biochemical experiments.

Internal Dynamics. The dynamic parameters were extracted using model-free analysis (*50–52*), and the axially symmetric diffusion model was used in the analysis. The calculations were performed using the experimentally determined relaxation data, their uncertainties, and the coordinates of the energy-minimized mean structures as input. The amide bond length was fixed at 1.02 Å, and a ^{15}N chemical-shift anisotropy value of –175 ppm was used in the calculations. Five increasingly complex models of internal mobility (M1, S^2; M2, S^2, τ_e; M3, S^2, R_{ex}; M4, S^2, τ_e, R_{ex}; and M5, S_f^2, S^2, τ_e) were iteratively used to reproduce the experimental data until the confidence reached within 95% (*52*). The confidence levels were estimated using 300 Monte Carlo simulations per run in combination with χ^2 and F statistic analysis. The optimized internal mobility parameters of the generalized order parameter S^2, the fast internal motion on pico-nanosecond timescales τ_e, and the conformational exchange R_{ex} on micro-millisecond timescales are shown in Figure 5B.

Residues in the regular secondary-structural elements were described mainly by M1 (except residues around the active site) with the average $S^2 = 0.85 \pm 0.04$ and 0.85 ± 0.04 for PspE in the sulfur-free and persulfide-intermediate forms, respectively. Residues Glu21, Glu50, Arg51, and Met99 in the sulfur-free form of PspE and Glu21, Glu50, Ala53, and Met99 in persulfide-intermediate form of PspE were assigned to M2 with the average $S^2 = 0.69 \pm 0.12$ and 0.69 ± 0.14 for the sulfur-free and persulfide-intermediate forms, indicating the internal motions (τ_e) on pico-nanosecond timescales. A total of 9 and 23 residues of the sulfur-free and persulfide-intermediate forms of PspE were assigned to M3, which showed the average $S^2 = 0.85 \pm 0.05$ and 0.84 ± 0.05 with average R_{ex} values of 4.2 and 10.7 Hz, respectively. No residues were assigned to M4 for both forms. One and three residues were assigned to M5 with the average $S^2 = 0.56 \pm 0.04$ and 0.45 ± 0.26 for sulfur-free and persulfide-intermediate forms of PspE, respectively.

The mapping of internal dynamic parameters onto PspE structures are shown in Figure 6. Overall, PspE in both forms show similar restricted motions on pico-nanosecond timescales as indicated by the high S^2 values. In addition, some regions in both forms also show micro-millisecond timescale conformational exchanges, especially around the active site. However, significant differences in dynamic properties were

observed between the two forms, especially the conformational exchanges on the micro-millisecond timescales. For the sulfur-free form of PspE, residues around the active site show millisecond conformational exchanges with an average R_{ex} of 4.2 Hz. In the persulfide-intermediate form, these residues exhibit micro-millisecond conformational exchanges, with an average R_{ex} of 10.7 Hz. Notably, there are more residues in the persulfide-intermediate form, showing micro-millisecond conformational exchanges, than the sulfur-free form of PspE, with larger R_{ex} values. On the other hand, the active residue Cys67 shows restricted internal motions in the sulfur-free form as reflected by the high S^2 value, while Cys67 shows a strong conformational exchange upon its binding to the substrate. These results indicate that the persulfide-intermediate form of PspE shows an overall enhanced conformational exchange compared to the sulfur-free form, which might be required for the next step of the reaction with cyanide. In the sulfur-free form of PspE, the restricted internal motion of Cys67 is mostly contributed by its hydrogen-bonding network with nearby residues. In the persulfide-intermediate form, however, the distances between the S_γ atom of Cys67 and its nearby residues mostly become larger. In contrast, the distances between the S_γ of Cys65 and the amide groups of the active-site residues (Tyr66, His67, Gly68, and Asn69) are 3.3, 4.0, 3.4, and 3.6 Å in the sulfur-free form of GlpE, while changed to 3.3, 3.8, 3.3, and 3.4 Å in the persulfide-intermediate form of GlpE (*13*). This may be an indication of more restricted internal motion in the persulfide-intermediate form of GlpE than its sulfur-free form. Subsequently, this may explain the previous experimental result that PspE shows a much higher activity than GlpE. Further investigations are required to address this issue.

Residues Arg27, His36, and Gly93, which are conserved among rhodaneses and located near the active site, show significant changes in internal dynamics between the sulfur-free and persulfide-intermediate forms of PspE. All of the three residues are described by model M1 in the sulfur-free form, while they are assigned to M3 with micro-millisecond conformational exchanges in the persulfide-intermediate form. Residues Arg27 and His36 have R_{ex} values of 2.0 ± 0.8 and 3.7 ± 0.5 Hz in the persulfide-intermediate form, respectively. Notably, Gly93 has a significantly high R_{ex} value (19.4 ± 1.1 Hz) in the persulfide-intermediate form, suggesting that the conservation of this residue in rhodaneses may be important for promoting the conformational flexibility of the active site during the enzymatic reaction. Interestingly, besides the active cysteine Cys67, the region Ala91−Ala98 show the most significant elevation in R_{ex} values when PspE is persulfurated. The residues in this region are all assigned to model M1 in the sulfur-free form, while in the persulfide-intermediate form, residues Ala91−Gly93, Lys95, and Ile97−Ala98 are assigned to M3, with an average R_{ex} of 12.9 Hz. In PspE, residue Gly93 is preceded by another two residues Ala91 and Gly92. These residues have intrinsic high flexibility and may strongly contribute to the increase of conformational exchanges at the active site in the persulfide-intermediate form of PspE. GlpE contains two Gly residues at the corresponding region (*13*), while bovine rhodanese and *A. vinelandii* rhodanese both contain only one Gly residue (*11, 12*). Whether these differences would affect the motional flexibility at the active site and consequently influence the enzymatic activities of these proteins remain to be further investigated.

Taken together, our observations on the internal dynamics of both forms of PspE are well-correlated to the catalytic reaction. For the sulfur-free form of PspE, the residues around the active site exhibit micro-millisecond conformational exchanges, which may contribute to the recognition of its substrate. Upon binding to the substrate, the persulfide-intermediate form of PspE shows overall enhanced conformational exchanges. Because the persulfide-intermediate form of PspE is a reaction intermediate, the enhanced conformational fluctuations on the micro-millisecond timescales is mostly likely required for its subsequent reaction with cyanide.

CONCLUSION

We have determined the structures of PspE in both sulfur-free and persulfide-intermediate forms, the first pair of solution structures of the rhodanese family. The structures reveal the detailed conformations of PspE in the prereaction and reaction intermediate states during the catalytic cycle. The structures in both forms indicate that there are no significant conformational changes during the rhodanese catalysis. In addition, it is well-known that the motional property plays a central role in enzyme catalysis. We investigated the backbone dynamics of PspE in both forms by NMR relaxation experiments. The results demonstrate that the dynamic properties of PspE in different forms, especially the change of motional properties, are well-coupled to each step of the catalytic reaction. Taken together, the present study indicates that not the change of conformations but the change of motional properties plays an essential role during the catalytic reaction of PspE. Therefore, our present study on structures in combination with the internal dynamics provides insightful information in understanding the catalytic mechanism of rhodanese.

ACKNOWLEDGMENT

All NMR experiments were carried out at the Beijing Nuclear Magnetic Resonance Center (BNMRC). We thank Dr. You Li, Yunfei Hu, and other members at BNMRC for their efforts in this project.

SUPPORTING INFORMATION AVAILABLE

HSQC spectra of PspE with and without DTT treatment (Figure S1). This material is available free of charge via the Internet at http://pubs.acs.org.

REFERENCES

1. Westley, J., and Heyse, D. (1971) Mechanisms of sulfur transfer catalysis. Sulfhydryl-catalyzed transfer of thiosulfonate sulfur. *J. Biol. Chem. 246*, 1468–1474.
2. Schlesinger, P., and Westley, J. (1974) An expanded mechanism for rhodanese catalysis. *J. Boil. Chem. 249*, 780–788.
3. Alexander, K., and Volini, M. (1987) Properties of an *Escherichia coli* rhodanese. *J. Biol. Chem. 262*, 6595–6604.
4. Westley, J. (1973) Rhodanese. *Adv. Enzymol. 39*, 327–368.
5. Westley, J., and Nakamoto, T. (1962) Mechanism of rhodanese action: Isotopic tracer studies. *J. Biol. Chem. 237*, 547–549.
6. Green, J. R., and Westley, J. (1961) Mechanism of rhodanese action: Polarographic studies. *J. Biol. Chem. 236*, 3047–3050.
7. Leininger, K. R., and Westley, J. (1968) The mechanism of the rhodanese-catalyzed thiosulfate-cyanide reaction. Thermodynamic and activation parameters. *J. Biol. Chem. 243*, 1892–1899.

8. Volini, M., and Westley, J. (1966) The mechanism of the rhodanese-catalyzed thiosulfate-lipoate reaction. Kinetic analysis. *J. Biol. Chem. 241*, 5168–5176.
9. Cipollone, R., Ascenzi, P., and Visca, P. (2007) Common themes and variations in the rhodanese superfamily. *IUBMB Life 59*, 51–59.
10. Bordo, D., and Bork, P. (2002) The rhodanese/Cdc25 phosphatase superfamily. Sequence-structure-function relations. *EMBO Rep. 3*, 741–746.
11. Ploegman, J. H., Drent, G., Kalk, K. H., Hol, W. G. J., Hienrikson, R. L., Keim, P., Wenig, L., and Russell, J. (1978) The covalent and tertiary structure of bovine liver rhodanese. *Nature 273*, 124–129.
12. Bordo, D., Deriu, D., Colnaghi, R., Carpen, A., Pagani, S., and Bolognesi, M. (2000) The crystal structure of a sulfurtransferase from *Azotobacter vinelandii* highlights the evolutionary relationship between the rhodanese and phosphatase enzyme families. *J. Mol. Biol. 298*, 691–704.
13. Spallarossa, A., Donahue, J. L., Larson, T. J., Bolognesi, M., and Bordo, D. (2001) *Escherichia coli* GlpE is a prototype sulfurtransferase for the single-domain rhodanese homology superfamily. *Structure 9*, 1117–1125.
14. Pantoja-Uceda, D., Lopez-Mendez, B., Koshiba, S., Inoue, M., Kigawa, T., Terada, T., Shirouzu, M., Tanaka, A., Seki, M., Shinozaki, K., Yokoyama, S., and Guntert, P. (2005) Solution structure of the rhodanese homology domain At4g01050 (175–295) from *Arabidopsis thaliana*. *Protein Sci. 14*, 224–230.
15. Hattori, M., Mizohata, E., Tatsuguchi, A., Shibata, R., Kishishita, S., Murayama, K., Terada, T., Kuramitsu, S., Shirouzu, M., and Yokoyama, S. (2006) Crystal structure of the single-domain rhodanese homologue TTHA0613 from *Thermus thermophilus* HB8. *Proteins 64*, 284–287.
16. Cornilescu, G., Vinarov, D. A., Tyler, E. M., Markley, J. L., and Cornilescu, C. C. (2006) Solution structure of a single-domain thiosulfate sulfurtransferase from *Arabidopsis thaliana*. *Protein Sci. 15*, 2836–2841.
17. Adams, H., Teertstra, W., Koster, M., and Tommassen, J. (2002) PspE (phage-shock protein E) of *Escherichia coli* is a rhodanese. *FEBS Lett. 518*, 173–176.
18. Model, P., Jovanovic, G., and Dworkin, J. (1997) The *Escherichia coli phage-shock-protein* (*psp*) operon. *Mol. Microbiol. 24*, 255–261.
19. Brissette, J. L., Russel, M., Weiner, L., and Model, P. (1990) Phage shock protein, a stress protein of *Escherichia coli*. *Proc. Natl. Acad. Sci. U.S.A. 87*, 862–866.
20. Darwin, A. J. (2005) The phage-shock-protein response. *Mol. Microbiol. 57*, 621–628.
21. Weiner, L., and Model, P. (1994) Role of an *Escherichia coli* stress-response operon in stationary-phase survival. *Proc. Natl. Acad. Sci. U.S.A. 91*, 2191–2195.
22. Adams, H., Teertstra, W., Demmers, J., Boesten, R., and Tommassen, J. (2003) Interactions between phage-shock proteins in *Escherichia coli*. *J. Bacteriol. 185*, 1174–1180.
23. Mittermaier, A., and Kay, L. E. (2006) New tools provide new insights in NMR studies of protein dynamics. *Science 312*, 224–228.
24. Eisenmesser, E. Z., Bosco, D. A., Akke, M., and Kern, D. (2002) Enzyme dynamics during catalysis. *Science 295*, 1520–1523.
25. Eisenmesser, E. Z., Millet, O., Labeikovsky, W., Korzhnev, D. M., Wolf-Watz, M., Bosco, D. A., Skalicky, J. J., Kay, L. E., and Kern, D. (2005) Intrinsic dynamics of an enzyme underlies catalysis. *Nature 438*, 117–121.
26. Palmer, A. G. (2004) NMR characterization of the dynamics of biomacromolecules. *Chem. Rev. 104*, 3623–3640.
27. Marley, J., Lu, M., and Bracken, C. (2001) A method for efficient isotopic labeling of recombinant proteins. *J. Biomol. NMR 20*, 71–75.
28. Sattler, M., Schleucher, J., and Griesinger, C. (1999) Heteronuclear multidimensional NMR experiments for the structure determination of proteins in solution employing pulsed field gradients. *Prog. Nucl. Magn. Reson. Spectrosc. 34*, 93–158.
29. Kay, L. E., Ikura, M., Tshudin, R., and Bax, A. (1990) 3-Dimensional triple-resonance NMR-spectroscopy of isotopically enriched proteins. *J. Magn. Reson. 89*, 496–514.
30. Wittekind, M., and Müller, L. (1993) HNCACB, a high-sensitivity 3D NMR experiment to correlate amide-proton and nitrogen resonances with the α-carbon and β-carbon resonances in proteins. *J. Magn. Reson. B 101*, 201–205.
31. Grzesiek, S., and Bax, A. (1993) Amino-acid type determination in the sequential assignment procedure of uniformly $^{13}C/^{15}N$-enriched proteins. *J. Biomol. NMR 3*, 185–204.
32. Grzesiek, S., Anglister, J., and Bax, A. (1993) Correlation of backbone amide and aliphatic side-chain resonances in $^{13}C/^{15}N$-enriched proteins by isotropic mixing of ^{13}C magnetization. *J. Magn. Reson. B 101*, 114–119.
33. Bax, A., Clore, G. M., Driscoll, P. C., Gronenborn, A. M., Ikura, M., and Kay, L. E. (1990) Practical aspects of proton carbon carbon proton 3-dimensional correlation spectroscopy of ^{13}C-labeled proteins. *J. Magn. Reson. 87*, 620–627.
34. Marion, D., Driscoll, P. C., Kay, L. E., Wingfield, P. T., Bax, A., Gronenborn, A. M., and Clore, G. M. (1989) Overcoming the overlap problem in the assignment of proton NMR spectra of larger proteins by use of three-dimensional heteronuclear proton-nitrogen-15 Hartmann-Hahn-multiple quantum coherence and nuclear Overhauser-multiple quantum coherence spectroscopy: Application to interleukin-1-β. *Biochemistry 28*, 6150–6156.
35. Delaglio, F., Grzesiek, S., Vuister, G. W., Zhu, G., Pfeifer, J., and Bax, A. (1995) NMRPipe—A multidimensional spectral processing system based on Unix pipes. *J. Biomol. NMR 6*, 277–293.
36. Johnson, B. A., and Blevins, R. A. (1994) NMR View—A computer-program for the visualization and analysis of NMR data. *J. Biomol. NMR 4*, 603–614.
37. Cornilescu, G., Delaglio, F., and Bax, A. (1999) Protein backbone angle restraints from searching a database for chemical shift and sequence. *J. Biomol. NMR 13*, 289–302.
38. Güntert, P., Mumenthaler, C., and Wüthrich, K. (1997) Torsion angle dynamics for NMR structure calculation with the new program DYANA. *J. Mol. Biol. 273*, 283–298.
39. Pearlman, D. A., Case, D. A., Caldwell, J. W., Ross, W. R., Cheatham, T. E., DeBolt, S., Ferguson, D., Seibel, G., and Kollman, P. (1995) Amber, a package of computer-programs for applying molecular mechanics, normal-mode analysis, molecular-dynamics and free-energy calculations to simulate the structural and energetic properties of molecules. *Comput. Phys. Commun. 91*, 1–41.
40. Herrmann, T., Guntert, P., and Wuthrich, K. (2002) Protein NMR structure determination with automated NOE assignment using the new software CANDID and the torsion angle dynamics algorithm DYANA. *J. Mol. Biol. 319*, 209–227.
41. Duggan, B. M., Legge, G. B., Dyson, H. J., and Wright, P. E. (2001) SANE (structure assisted NOE evaluation): An automated model-based approach for NOE assignment. *J. Biomol. NMR 19*, 321–329.
42. Koradi, R., Billeter, M., and Wuthrich, K. (1996) MOLMOL: A program for display and analysis of macromolecular structures. *J. Mol. Graphics 14*, 29–32.
43. Laskowski, R. A., Rullmannn, J. A., MacArthur, M. W., Kaptein, R., and Thornton, J. M. (1996) AQUA and PROCHECK-NMR: Programs for checking the quality of protein structures solved by NMR. *J. Biomol. NMR 8*, 477–486.
44. Farrow, N. A., Muhandiram, R., Singer, A. U., Pascal, S. M., Kay, C. M., Gish, G., Shoelson, S. E., Pawson, T., Forman-Kay, J. D., and Kay, L. E. (1994) Backbone dynamics of a free and a phosphopeptide-complexed SRC homology-2 domain studied by ^{15}N NMR relaxation. *Biochemistry 33*, 5984–6003.
45. Fushman, D., Cahill, S., and Cowburn, D. (1997) The main-chain dynamics of the dynamin pleckstrin homology (PH) domain in solution: Analysis of ^{15}N relaxation with monomer/dimer equilibration. *J. Mol. Biol. 266*, 173–194.
46. Mueller, E. G. (2006) Trafficking in persulfides: Delivering sulfur in biosynthetic pathways. *Nat. Chem. Biol. 2*, 185–194.
47. Holm, L., and Sander, C. (1993) Protein structure comparison by alignment of distance matrices. *J. Mol. Biol. 233*, 123–138.
48. Cicero, D. O., Melino, S., Orsale, M., Brancato, G., Amadei, A., Forlani, F., Pagani, S., and Paci, M. (2003) Structural rearrangements of the two domains of *Azotobacter vinelandii* rhodanese upon sulfane sulfur release: Essential molecular dynamics, ^{15}N NMR relaxation and deuterium exchange on the uniformly labeled protein. *Int. J. Biol. Macromol. 33*, 193–201.
49. Dosset, P., Hus, J. C., Blackledge, M., and Marion, D. (2000) Efficient analysis of macromolecular rotational diffusion from heteronuclear relaxation data. *J. Biomol. NMR 16*, 23–28.
50. Lipari, G., and Szabo, A. (1982) Model-free approach to the interpretation of nuclear magnetic-resonance relaxation in macromolecules. 1. Theory and range of validity. *J. Am. Chem. Soc. 104*, 4546–4559.
51. Lipari, G., and Szabo, A. (1982) Model-free approach to the interpretation of nuclear magnetic-resonance relaxation in macromolecules. 2. Analysis of experimental results. *J. Am. Chem. Soc. 104*, 4559–4570.

52. Mandel, A. M., Akke, M., and Palmer, A. G. (1995) Backbone dynamics of *Escherichia coli* ribonuclease HI—Correlations with structure and function in an active enzyme. *J. Mol. Biol. 246*, 144–163.
53. Michalopoulos, I., Torrance, G. M., Gilbert, D. R., and Westhead, D. R. (2004) TOPS: An enhanced database of protein structural topology. *Nucleic Acid Res. 32*, D251–D254.
54. Mukder, F. A. A., Schipper, D., Bott, R., and Boelens, R. (1999) Altered flexibility in the substrate-binding site of related native and engineered high-alkaline *Bacillus subtilisins*. *J. Mol. Biol. 292*, 111–123.

BI800039N